Minerals Engineering 196 (2023) 108048

Contents lists available at ScienceDirect

Minerals Engineering

journal homepage: www.elsevier.com/locate/mineng

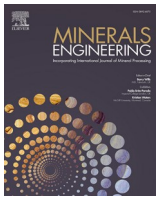

Towards sustainable mass production of metallic nanoparticles: Selective synthesis of copper nanoparticles directly from malachite ore

R.A. Crane [a,*], D.J. Sapsford [b]

[a] Camborne School of Mines, College of Engineering, Mathematics and Physical Sciences, University of Exeter, Penryn Campus, Penryn, Cornwall TR10 9FE, United Kingdom
[b] School of Engineering, Cardiff University, Queen's Building, The Parade, Cardiff CF24 3AA, United Kingdom

ARTICLE INFO

Keywords:
Cementation
Chemical reduction
Hydrometallurgy
Valorisation
Upcycling

ABSTRACT

Continuing industrial development and burgeoning pressure to solve global challenges, including climate change and non-pharmaceutical pathogen management, will drive an urgent up-scaling in global nanoparticle production this Century. Conventional nanoparticle synthesis is typically a linear multistage approach comprising mining, beneficiation, refining, reagent synthesis and then nanoproduct synthesis, which is both energy and resource intensive. Herein, we present a new approach using nanoscale Cu (nCu) as an example of the translocation of nanoparticle synthesis into the subsurface in one step. Malachite ore was first leached with H_2SO_4 or CH_3COOH (0.5 M, 1:10 solid–liquid ratio), partially neutralised using 0.01–0.5 M NaOH or $NaCO_3$ respectively and then exposed to nanoscale zerovalent iron (nZVI) (4.0 g/L). The nZVI acted as both a selective and rapid (<240 s) chemical reducing agent but also a magneto-responsive nCu recovery vehicle. Up to 31.1 wt% conversion of Cu from ore to discrete Cu^0/Cu_2O nanoparticles was observed, with nanoparticle purities of up to 81.70 wt% Cu (or 98.59 wt% Cu and O) detected using HRTEM. This work therefore provides a first proof-of-concept of a new direct and one-pot "*in situ*" nanoparticle mass production route. This routeis conceptually feasible for a wide range of engineered nanomaterials, including those containing Ni, Cr, U, Pb, Ag and Au, and therefore has the potential to yield transformative environmental and economic benefit across mining and raw material synthesis industries.

1. Introduction

Metallic nanoparticles have a vital role in enabling technological solutions for global challenges of the 21st century. There is a compelling case for the development of sustainable routes for mass production of these materials to enable key applications. The include use in chemical synthesis, closing the carbon cycle, improving agricultural productivity and non-pharmaceutical antimicrobials for countering the concurrent threat of global pandemics and the growing prevalence of drug-resistant pathogens. Some pertinent examples for copper, copper (I) and copper (II) oxides nanoparticles (hereafter referred to as nCu) are briefly expounded, as follows.

1.1. Applications of nCu

Gawande et al (Gawande et al., 2016) (Gawande et al., 2016) outline the wider range of applications of nanoscale Cu/CuOx catalysts including in reduction, oxidation, A3-coupling, electrocatalysis, photocatalysis and gas-phase reactions. CO_2 utilisation as a chemical feedstock is a major plank of a global strategy for closing the carbon loop to combat climate change. The electrochemical reduction of CO_2 to useful products including formic acid, methanol, syngas and higher hydrocarbons (Jones et al., 2014) is an attractive route to achieve this. The technology is enabled by use of metallic catalysts, of which nanoparticulate/nanostructured Cu/CuO is recognised as being particularly promising because of high Faradic efficiencies and low overpotentials (Xie et al., 2018).

Cu, particularly when applied as nCu, has long been recognised as an antimicrobial, demonstrating bactericidal, fungicidal and viricidal activity (Ingle et al., 2014); (Jardón-Maximino et al., 2021); (Jardón-Maximino et al., 2021). Specific examples include efficacy against pathogenic bacteria such as *Staphylococcus aureus*, fungi such as *Candida albicans*, and the influenza virus (Ameh and Sayes, 2019). Potential applications include utilisation or incorporation of nCu into food

* Corresponding author.
E-mail address: r.crane@exeter.ac.uk (R.A. Crane).

https://doi.org/10.1016/j.mineng.2023.108048
Received 15 March 2022; Received in revised form 23 February 2023; Accepted 27 February 2023
Available online 14 March 2023

packaging, personal protective equipment, water disinfection, for control of biofouling in membrane applications and in antimicrobial composites, coatings and textiles (Ogunsona et al., 2020).

The global population is projected to approach 10 billion by 2050 with a commensurate increase in food demand (Foley et al., 2011); (Mueller et al., 2012). In this context, nCu could be a key material in sustainable agriculture. Agritech applications of nCu include as fungicides (Ponmurugan et al., 2016), improvement of nutrient-use and nitrogen-fixation (Guan et al., 2020) and in combatting salt stress (González-García et al., 2021). For example, nCu have been shown to increase the growth of soybean under field conditions (Ngo et al., 2014) and may even have a role in the biofortification of crops, particularly those grown on alkaline soils (Dimkpa et al., 2012).

Other examples of the vast range of potential applications of nCu include as an additive for improved emission from combustion of fuels e.g. biodiesel (Tamilvanan et al., 2019); in conductive inks (Zhang et al., 2014); additives in lubricants (Borda et al., 2018); and as a cooling water additive for improvement of heat conductivity (Slotte and Zevenhoven, 2017).

1.2. Conventional nCu synthesis routes

The large-scale and range of applications outlined above require commensurate means of sustainable and economical nCu mass-production which will otherwise curb the uptake of these transformative technologies.

Current batch synthesis methods include electrochemical deposition (Yuan et al., 2007), hydrothermal (Neupane et al., 2009); (Outokesh et al., 2011), precipitation (Zhu et al., 2004), microwave assisted (Nikam et al., 2014), solid state synthesis (Vidyasagar et al., 2012) and mechanochemical synthesis (Baláž et al., 2020). Other methods recently explored include the green synthesis of nCu which have been anchored onto filtration media (Pérez-Alvarez et al., 2021) and novel approaches for the synthesis of nCu which is resistant to oxidation (Jardón-Maximino et al., 2018). Continuous/larger-scale production has been achieved using arc/spark methods (e.g. (Ngo et al., 2014) and Continuous Hydrothermal Flow Synthesis (CHFS) using supercritical water (Gupta et al., 2016), which when combined with confined jet mixer, is reported to yield kg/day quantities (Elouali et al., 2012). It is clear that there is currently a substantial mismatch between the scale of production reported in the literature and the very large amounts of nCu needed to meet the range of future industrial applications.

In terms of environmental sustainability, it is acknowledged that Life Cycle Assessment studies on nanomaterials production are scarce (Ngo et al., 2014). However, regardless of the nCu synthesis method chosen, there are already substantial "in-built" environmental footprints associated with the original production of the precursor Cu reagents (i.e. starting with mining and beneficiation of Cu from its ore.This is then followed by a series of purification and chemical engineering steps in order to yield the final Cu reagent raw material, usually as water soluble salt).

In 2018, more than 99% of the mass of all metals and metalloids were extracted from the Earth using physical excavation mining methods, with the vast majority *via* open cast methods (Seredkin et al., 2016 Dec). It is by definition an invasive process and requires the complete physical extraction of surface soil and overburden rock (and associated biota), in order to gain access to the ore. The ore then invariably requires beneficiation through removal of gangue material (often > 90 % by volume) at a purpose-built facility. Overall the process results in staggeringly large quantities of solid waste; currently averaging 20–25 billion tonnes per year, which is approximately 20 times larger than all global municipal waste generation (https://openknowledge.worldbank.org/handle/10986/30317). On the local and regional scale adverse effects have included major and irreversible habitat destruction, pollution of ground and surface waters with ecotoxic metals and/or acidic/alkaline pH mine water, and the aeolian migration of ecotoxic dust over vast distances (Hudson-Edwards et al., 2011). Such factors can jeopardise the social license of mining companies to operate and when poorly managed, mines can cause major negative impacts to human health and ecosystems. Because of the large energy requirements of transporting, crushing and processing billions of tonnes of material, mining remains one of the most significant individual industrial contributors to global CO_2 emissions. Sustainable routes to the mass production of nCu therefore need to include ways to minimise the lifecycle impacts from cradle to grave and this begins with sustainable mining practices (Martens et al., 2021).

1.3. Use of nZVI as a selective reducing agent for sustainable nCu production

This work has been established in order to provide a proof of concept for the application of nanoscale zerovalent iron particles (nZVI) as a magneto-responsive chemical reducing agent for the selective recovery of Cu from its parent ore. Cu is higher on the galvanic series than Fe and as such exhibits well-known utility in the reductive precipitation of Cu from the aqueous phase (Reaction (1)) (Crane and Sapsford, 2018 Apr).

$$Fe^{0}_{(s)} + Cu^{2+}_{(aq)} = Fe^{2+}_{(aq)} + Cu^{0}_{(s)} \; E^{0} = 0.78 \text{ V} \quad (1)$$

Several common metals also exhibit lower standard electrode potentials (E^0) for their reduction to a metallic state than Fe^{2+} (−0.44 V), including: K^+ (−2.92 V), Ca^{2+} (−2.84 V), Na^+ (−2.71 V), Mg^{2+} (−2.37 V), Mn^{2+} (−1.18 V) and Zn (−0.76 V), and therefore often remain in the aqueous phase when exposed to Fe^0. This enables the Fe-Cu cementation reaction to be highly selective (Zhu et al., 2004). Whilst bulk scale Fe^0 has been widely tested for such applications (Stefanowicz et al., 1997 Nov 1), until now very little is currently known with regard to the comparative efficacy of nZVI and also the physicochemical properties of resultant Cu-bearing (nano)precipitates. Whilst the superior specific surface area of nZVI enables fast reaction kinetics its transformative potential is likely due to its nanometer scale.When combined with its (super)paramagnetic behaviour and ability to act as a ferrofluid, this unlocks the potential to enable *in situ* (i.e. subsurface or "in-pulp") injection of nZVI into a target zone (e.g. a leached high grade ore body) followed by *in situ* nCu synthesis and magnetic recovery. The net result therefore is the direct and one-step "translocation of nCu synthesis into the subsurface", which could thereby enable a move beyond the current linear and multistep paradigm of mining, beneficiation, refining, Cu-reagent synthesis and nCu product synthesis.

2. Methodology

2.1. nZVI synthesis

Pure nZVI nanoparticles were synthesised following the methodology first described by Glavee et al., (Glavee et al., 1995) and then adapted by Wang and Zhang (Wang and Zhang, 1997). 7.65 g of $FeSO_4{\cdot}7H_2O$ was dissolved in 50 mL of Milli-Q water (>18.2 MΩ cm) and the pH was adjusted to 6.8 using 4 M NaOH. NaOH addition was performed slowly, drop-wise, to avoid the formation of hydroxo-carbonyl complexes. The salts were reduced to nZVI by the addition of 3.0 g of $NaBH_4$. The nanoparticle product was isolated from the aqueous phase via centrifugation (Hamilton Bell v6500 Vanguard centrifuge, 6500 RPM for 120 s), rinsed with absolute ethanol (Fisher Scientific, 12478730; ratio of 50 mL/g of nZVI) and then centrifuged (Hamilton Bell v6500 Vanguard centrifuge, 6500 RPM for 120 s). This step was then repeated three more times. The nanoparticles were dried in a vacuum desiccator (approx. 10^{-2} mbar) for 72 h and then stored in an argon filled (BOC, 99.998 %) MBraun glovebox until required.

2.2. nCu synthesis experiments

Malachite ore was obtained from a major Cu mine in the USA and was crushed (to particle size < 75 μm), using a Labtech Essa LM1-P puck mill crusher at 935 RPM for 120 s, in order to ensure homogeneity for the subsequent nCu synthesis experiments.

The nCu synthesis experiments were conducted by exposing 40 mL aliquots of either sulfuric (H_2SO_4) or acetic acid (CH_3COOH) to 4 g of the Cu ore whilst being constantly mixed at 100 Revolution Per Minute (RPM) using a Stuart SSL1 orbital shaker table for fixed time periods. These acids were selected in order to compare the efficacy of a strong acid with a weak acid respectively. Sulfuric acid was also selected because it is the most common reagent currently used for commercial malachite leaching (Bingöl and Canbazoğlu, 2004). Acetic acid was also selected because it is readily biodegradable and as such potentially more suitable than sulfuric acid for *in situ* applications (Crane and Sapsford, 2018 Sep). A 10 mL sample of the crushed ore acid slurry was then extracted from each batch system using an autopipette and centrifuged at 4000 RPM (3077 *g*) for 240 s (Sigma 3–16 L centrifuge). The supernatant was then extracted using a 10 mL syringe and filtered through a cellulose acetate filter 0.2 μm filter. The filtrate was collected for ICP-OES analysis. 10 mL of either NaOH or $NaCO_3$ were then added to the batch systems containing sulfuric (H_2SO_4) and acetic acid (CH_3COOH) respectively. NaOH and $NaCO_3$ were selected for use as neutralising agents for the H_2SO_4 or CH_3COOH leached Cu ore samples respectively. This wasin order to compare the different behaviour (and associated impact on Cu removal efficacy) of strong acid and strong base combinations with weak acid and weak base combinations. The concentrations added were: 0.04, 0.4, 0.8, 1.6 and 2.0 NaOH or $NaCO_3$, which created an overall concentration within the vial of 0.01, 0.1, 0.2, 0.4 and 0.5 M NaOH or $NaCO_3$. The batch systems were each mixed at 100 RPM (Stuart SSL1 orbital shaker table) for 240 s. A 10 mL sample of the slurry was then taken and centrifuged at 4000 RPM (3077 *g*) for 240 s (Sigma 3–16 L centrifuge). The supernatant was then extracted using a 10 mL syringe and filtered through a cellulose acetate filter 0.2 μm filter.The filtrate collected for ICP-OES analysis. nZVI was then added to each batch system at a concentration of 4.0 g/L (0.12 g). The batch systems were than mixed at 100 RPM (Stuart SSL1 orbital shaker table) for 240 s. A 10 mL sample of the slurry was then taken from each batch system and centrifuged at 4000 RPM (3077 *g*) for 240 s (Sigma 3–16 L centrifuge). The supernatant was then extracted using a 10 mL syringe and filtered through a cellulose acetate filter 0.2 μm filter for ICP-OES analysis. The residual nZVI was then extracted from each system using an Eclipse 20 mm Neodymium Pot Magnet (length 25 mm, pull force 28 kg) which was covered in a single layer of Parafilm (Fisher Scientific, 11762644). The Parafilm was then removed from the magnet and the residual nZVI collected into a 50 mL polypropylene centrifuge tube (Fisher Scientific, 11512303). 30 mL of absolute ethanol (Fisher Scientific, 12337163) was then added and the nZVI-ethanol slurry then gently agitated by hand. The centrifuge tube was then centrifuged at 4000 RPM (3077 *g*) for 240 s and the supernatant then decanted. This ethanol washing procedure was then repeated twice more. The centrifuged nZVI plug was then pipetted onto a glass optical microscope slide (Agar Scientific, G251P) for XRD and a Au coated holey carbon film (TAAB, C062/G) for HRTEM and FEG-SEM analysis. Samples were stored in an argon filled (BOC, 99.998%) MBraun glovebox until required for such analysis. During their transfer into the XRD or TEM/SEM instruments careful examination of the colour of the sample was noted (in order to account for any oxidation). No colour change was noted which indicates that once dry the samples were stable. All experiments were conducted at room temperature (measured to be 20.0 °C ± 1.0 °C) and ran as duplicate pairs, with the average data used to create the figures/tables displayed herein. All mass balance calculations were calculated by comparing the mass of each metal leached into the dissolved phase (recorded using ICP-OES) with the original mass of such metals in the original Cu ore sample.

2.3. Analytical techniques

A Phillips Xpert Pro diffractometer with a CoKa radiation source was used for X-Ray Diffraction (XRD) analysis (generator voltage of 40 keV; tube current of 30 mA). XRD spectra were acquired between 2 h angles of 10–90°, with a step size of 0.02° 2 and a 2 s dwell time. Acid digestion was conducted using a 4-acid microwave digest (EPA, 1996). Firstly, 0.01 g was placed in a Polytetrafluoroethylene (PTFE) lined microwave digest cell and 3 mL of analytical grade 45.71 % hydrofluoric acid (HF) was then added and left for 12 hrs. 6 mL of aqua regia solution (1:1 ratio of analytical grade 32 % hydrochloric acid (HCl) and 70 % nitric acid (HNO_3)) was then added and the container was then placed in a microwave digest oven (Anton Paar Multiwave 3000) and heated at 200 °C (1400 W) for 30 min (after a 10 min up ramp time period) and then allowed to cool for 15 min. The resultant solution was then neutralised using 18 mL of analytical grade 4 % Boric acid (H_3BO_3) at 150 °C (900 W) for 20 min (after a 5 min up ramp time period) and then allowed to cool for 15 min. Inductively coupled plasma-optical emission spectroscopy (ICP-OES) analysis was performed using a Perkin Elmer Optima 2100 DV ICP-OES. High-resolution transmission electron microscopy (HRTEM) analysis was performed using a JEOL JEM-2100 microscope at 200 kV. Field emission gun scanning electron microscope (FEG-SEM) analysis was performed using a Tescan MAIA-3 FEG-SEM. Energy dispersive spectroscopy (EDS) analysis and mapping was performed using Oxford Instruments X-MaxN analyzer and Aztec software. A beryllium sample holder and Au grids were used in order to prevent any background Cu from being detected. Nanoparticle size distribution from HRTEM images was measured using ImageJ software (Java 1.6.0_24) with 100 nanoparticles analysed per sample.

3. Results and discussion

3.1. Characterisation of the as-formed nZVI

HRTEM analysis determined that the nZVI were spherical with an average diameter of 61 nm and a particle size distribution as follows: <50 nm: 32.1 %, 50–100 nm: 58.5 %, >100 nm: 9.4 % (Fig. 1). Each individual nZVI particle was recorded to contain a discrete outermost layer (density contrast), which is attributed to be the presence of an oxide shell surrounding the Fe^0 core. In addition, dark mottles were recorded within the metallic cores which indicates that individual particles were either polycrystalline or comprised isolated metal crystals in an otherwise amorphous matrix. Individual nZVI particles were aggregated into chains and rings due to their high surface energy and magnetic properties (Baalousha, 2009); (Crane and Sapsford, 2018 Aug). The surface area of the nZVI was determined using Brunauer–Emmett–Teller (BET) surface area analysis as 50.9 m^2/g. XRD analysis recorded a single relatively broad diffraction peak at 52.381° 2θ which was attributed to the (1 1 0) lattice reflection of α-Fe^0 (Nikam et al., 2014). Overall the physicochemical characteristics of the nZVI were consistent with previous studies who have used borohydride precipitated nZVI (e.g. (Scott et al., xxxx); (Crane et al., xxxx); (Crane et al., xxxx); (Crane and Scott, 2013); (Vilardi, 2019)).

3.2. Characteristics of the Cu ore

XRD determined the major crystalline component of the ore mineral as malachite ($Cu_2CO_3(OH)_2$) within minor concentrations of dolomite ($CaMg(CO_3)_2$), and quartz (α-SiO_2) (Fig. 2). This corroborates with the elemental composition data (Table 2), which show that Ca, Cu and Mg are among the most abundant metal elements in the ore.

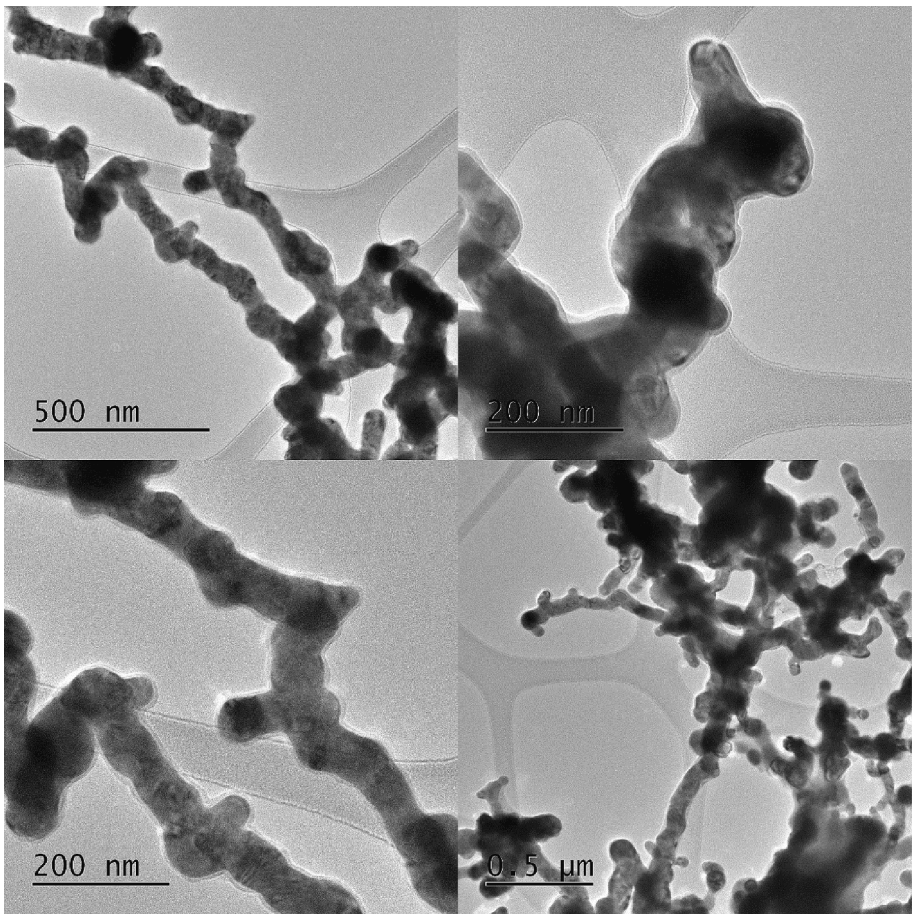

Fig. 1. HRTEM images of the as-formed nZVI.

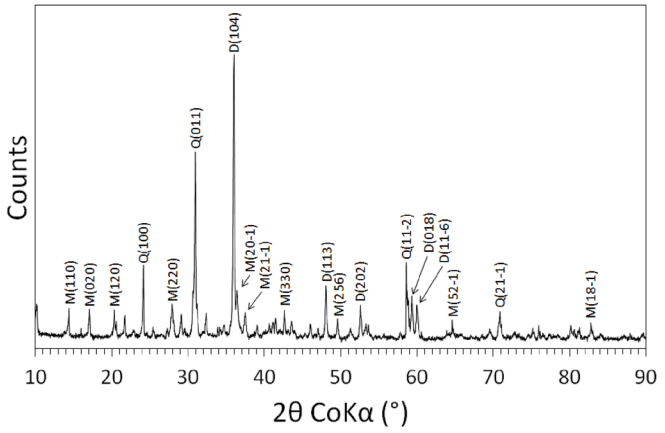

Fig. 2. XRD profile for the as-received Cu ore. The peaks identified as dolomite, quartz and malachite are denoted as D, Q and M respectively.

3.3. Aqueous metal concentration data for the ore leaching step and the nanoparticle synthesis step

Fig. 3 displays percentage dissolution of Cu from its ore following exposure to H_2SO_4 or CH_3COOH at 0.01–1 M and 0.1–4 M respectively. Cu dissolution was 0.1, 28.3, 67.4 and 80.0 wt% using H_2SO_4 at 0.01, 0.1, 0.5 and 1.0 M respectively. H_2SO_4 or CH_3COOH concentration of 0.5 M was therefore selected for the subsequent nCu synthesis experiments (Fig. 4) because it represents a relatively good balance between high wt.% Cu dissolution from the ore, whilst also still being a relatively low concentration (i.e. relatively environmentally benign). In these systems considerable Cu was dissolved from ore samples by both 0.5 M H_2SO_4 and CH_3COOH. The H_2SO_4 was more effective, with average Cu dissolution of 65.9 wt% compared to 15.0 wt% respectively. Both acids were also selective for Cu dissolution compared to the other metals (Table 1) but did dissolve relatively high proportions of Ca: 5.6 wt% and 10.6 wt% respectively. H_2SO_4 also dissolved a relatively high concentrations of Fe (20.0 wt% dissolved) and Mg (44.5 wt% dissolved). As such it can be stated that both acids were relatively selective for Cu, but despite its lower efficacy, CH_3COOH was more selective than H_2SO_4.

Fig. 4 displays percentage dissolution of Cu using 0.5 M H_2SO_4 (top) or CH_3COOH (bottom) (dashed lines) after which different concentrations of NaOH or $NaCO_3$ were respectively added (square markers). The leachates were then exposed to the nZVI (circle markers). NaOH addition to the H_2SO_4 leached solutions did not prevent further Cu dissolution, which is attributed to only partial neutralisation of the acid. Additional Cu dissolution was also recorded following the addition of 0.01 and 0.1 M $NaCO_3$ and in contrast precipitation was recorded following the addition of 0.2, 0.4 and 0.5 M $NaCO_3$. This corroborates well with the theoretical equivalence concentration of 0.25 M $NaCO_3$ in order to neutralise 0.5 M CH_3COOH.

In all systems the addition of the nZVI resulted in the removal of Cu from solution, with the mechanism attributed to be the selective cementation of aqueous Cu with Fe^0 (Reaction (1)). No clear relationship was determined between such Cu removal for the ore samples which had been leached with 0.5 M H_2SO_4 and then neutralised using NaOH (0.1–0.5 M), with 28.0, 24.5, 26.3, 31.0 and 29.6 wt% of the total leached Cu being converted to precipitate for the batch systems neutralised using NaOH at 0.01, 0.1, 0.2, 0.4 and 0.5 M respectively (as indicated by the orange colour in Fig. 4). In contrast, an inverse

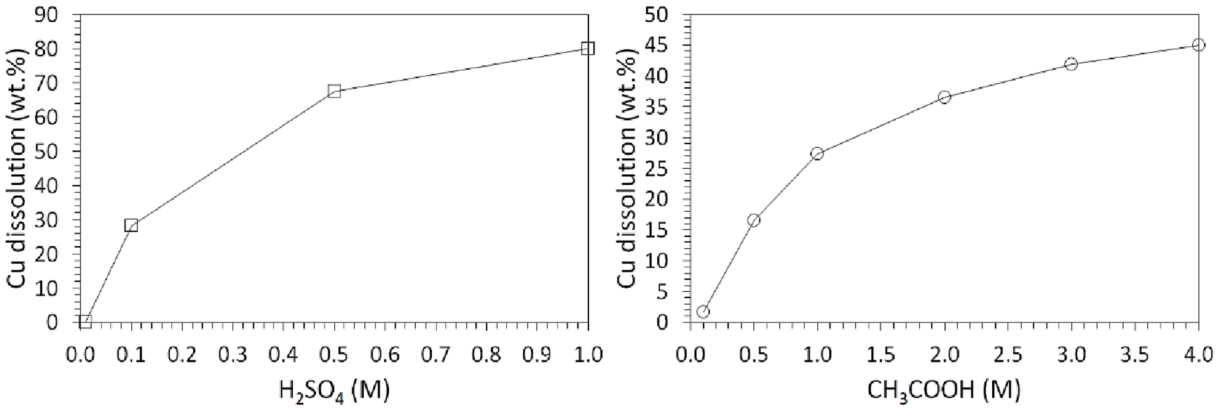

Fig. 3. Cu dissolution (expressed as wt. % of original Cu content) from the Cu ore as a function of H_2SO_4 or CH_3COOH concentration. Experiments used a 10:1 liquid solid ratio, 100 RPM constant mixing intensity and a leaching time of 2 hrs.

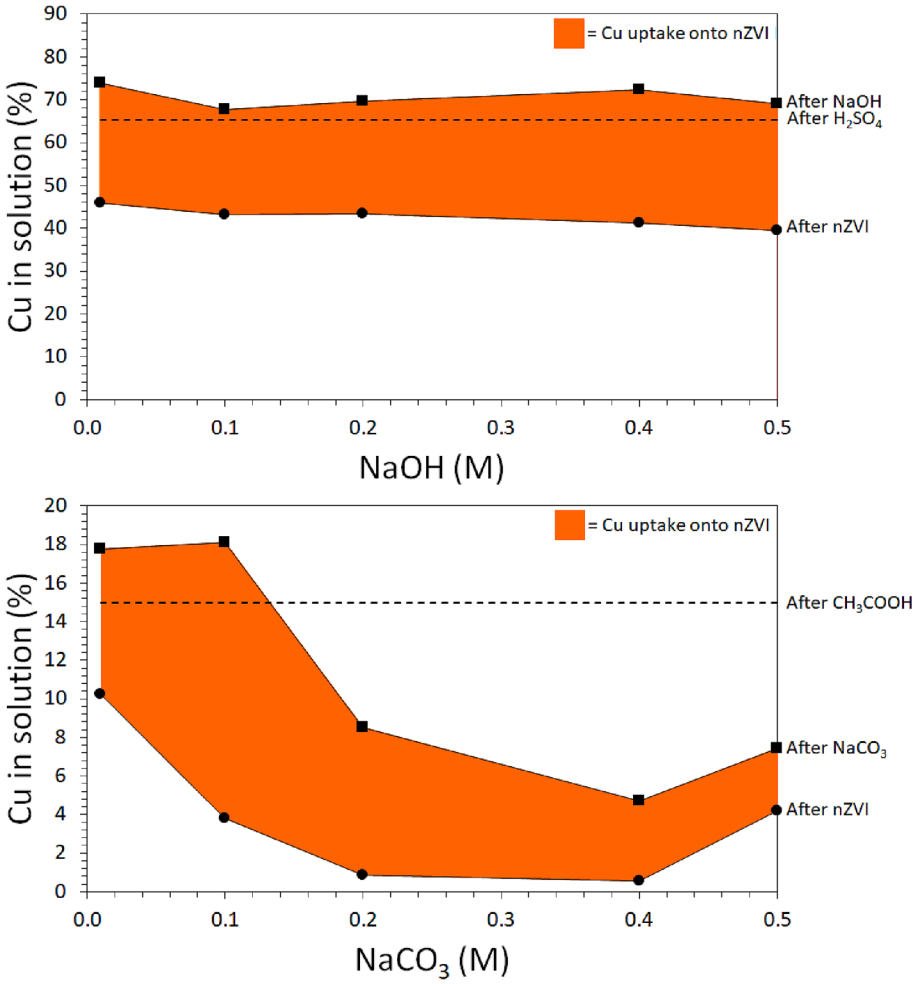

Fig. 4. The proportion of aqueous Cu (relative to the total in the ore) following acid leaching (0.5 M H_2SO_4 or CH_3COOH) for 2 h then partial neutralisation (0.01–0.5 M NaOH or $NaCO_3$) for 900 s and then nZVI addition (4.0 g/L) for 240 s. A 10:1 liquid solid ratio of lixiviant to ore was maintained throughout.

correlation in Cu removal onto nZVI was recorded for ore samples that were leached using 0.5 M CH_3COOH and then neutralised using $NaCO_3$ (0.1–0.5 M), with maximum Cu removal onto nZVI of 14.32 wt% recorded for the batch system neutralised using 0.1 M $NaCO_3$ compared to 7.65, 4.13 and 3.23 wt% recorded for systems neutralised using 0.2, 0.4 and 0.5 M $NaCO_3$.

Table 2 displays the average relative proportion (wt. %) of aqueous metals recorded in the leachates (i.e. before nZVI was added) against those in the "removed phase" i.e. after nZVI was added. Within this all concentrations were calculated using mass balance from the ICP-OES data.The "leachate" was calculated using aqueous metal concentrations in the leachate before nZVI addition. The "removed phase" was calculated using aqueous metal concentrations in the leachate before nZVI addition minus their concentrations in the leachate following nZVI addition).

H_2SO_4 (after partial neutralisation using NaOH) was more effective

Table 1
Metal composition (wt.%) of the Cu ore (determined using ICP-OES analysis following total acid digestion) and the average wt.% extraction of each element using 0.5 M H_2SO_4 and CH_3COOH (SL ratio: 1:10, mixing time: 2 hrs). Minor concentrations (<0.1 wt%) were also recorded for Zn, Ag, Co, Mn, Cr, Ni, Pb, Li, Sr and Mo.

	wt. %	0.5 M H_2SO_4	0.5 M CH_3OOH
Al	2.459	2.8	0.2
K	1.190	3.8	1.0
Ca	8.869	5.6	10.6
Fe	1.894	20.0	0.7
Ti	0.129	1.0	0.1
Cu	8.069	67.4	16.6
Na	0.537	0.5	0.4
Mg	5.863	44.5	3.1

Table 2
Average relative proportion of metals* (wt. %) recorded in the "leachate" and the "removed phase". The "leachate" was formed due to the exposure of Cu ore to 0.5 M H_2SO_4 or CH_3COOH (for 2 h) followed by partial neutralisation using 0.01–0.5 M NaOH or $NaCO_3$ (for 900 s). A 10:1 liquid solid ratio of lixiviant to ore was maintained throughout. The "removed phase" was formed due to the addition of nZVI at 4.0 g/L for 240 s. *Zn, Ag, Co, Cr, Ti, Ni, Li, Sr were also analysed but recorded as less than detection limit.

	H_2SO_4 + NaOH + nZVI		CH_3COOH + $NaCO_3$ + nZVI	
	Relative proportion of metals (wt. %) in the leachate	Relative proportion of metals (wt. %) in the removed phase (following nZVI addition)	Relative proportion of metals (wt.%) in the leachate	Relative proportion of metals (wt. %) in the removed phase (following nZVI addition)
Al	0.5	0.0	0.0	0.1
K	0.3	0.0	0.1	0.0
Ca	7.9	5.1	6.3	1.0
Fe	1.8	0.0	0.1	0.0
Mn	0.1	0.0	0.0	0.0
Cu	50.0	94.9	11.7	97.5
Sb	0.1	0.0	0.1	0.4
Pb	0.1	0.0	0.1	0.2
Na	19.1	0.0	79.6	0.2
Mg	20.2	0.0	2.0	0.5
Mo	0.0	0.0	0.0	0.1
Total	100	100	100	100

for Cu dissolution than CH_3COOH (after neutralisation using $NaCO_3$) with Cu comprising 50.0 wt% of the total dissolved metals in the leachate compared to 11.7 wt% respectively, with the remainder of the latter leached phase dominated by Na (presumably largely derived from $NaCO_3$).

Following nZVI addition Cu was calculated as comprising 94.9 wt% of the removed metal load for the H_2SO_4 system whilst 97.5 wt% for the CH_3COOH system. It can therefore be stated that nZVI was highly selective for Cu removal from both systems, but slightly more selective from the CH_3COOH system.

3.4. Crystalline composition of the synthesised nanoparticles

Fig. 5 displays XRD data for nZVI which were magnetically extracted from the leached Cu ore samples (leached using 0.5 M H_2SO_4 (Left Hand Side (LHS)) or CH_3COOH (Right Hand Side (RHS)) after they were partially neutralised using NaOH or $NaCO_3$ respectively). Peaks corresponding to Cu^0 were recorded for all samples which confirms that the removal mechanism of aqueous Cu onto nZVI was *via* cementation (Reaction (1)). Cu_2O was also detected in common with other studies of Cu^{2+} uptake on nZVI (e.g. (Karabelli et al., 2008); (Li et al., 2014); (Liu et al., 2022)), presumably from the oxidation of Cu^0. Fe^0 was recorded as the sole crystalline iron-bearing phase for all samples (no crystalline iron corrosion phases identified), which suggests that remaining unreacted nZVI could be recycled in the process. Fe^0 was the most prominent crystalline phase detected for Cu-bearing leachates which had been neutralised with a higher concentration of neutralising agent (base).This highlights the requirement for pH neutralisation, which limits dissolution of the nZVI (which is required in order to assist in the magnetic recovery of nCu). In contrast for the lower base concentrations, the final product comprised very little Fe^0 and was therefore a more chemically pure nCu product. This product would be beneficial if there were no requirement to reuse the nZVI or utilise magnetic recovery in a process using these reactions. Minor contributions from quartz (both systems) and dolomite (only the CH_3COOH and $NaCO_3$ systems) were also identified in the samples, which is attributed to the co-removal of fragments of mineral fines, within Cu and/or Fe^0 bearing nanoparticles.

3.5. Shape, particle size distribution and elemental composition of the synthesised nanoparticles

FEG-SEM images (and corresponding EDS maps for the three most abundant metals detected) of the nCu produced due to the exposure of nZVI to the leached Cu ore slurry (leached using 0.5 M H_2SO_4 or CH_3COOH and then neutralised using 0.1 M NaOH (Fig. 6) or $NaCO_3$ (Fig. 7) respectively) show that in both scenarios the nanomaterial synthesised was predominantly discrete nanoparticles containing Cu and O. In particular, EDS analysis show that the nanoparticles were 81.70 wt% Cu (98.59 % Cu and O) and 77.60 wt% Cu (88.73 wt% Cu and O) for those derived from Cu ore slurry which was leached using 0.5 M

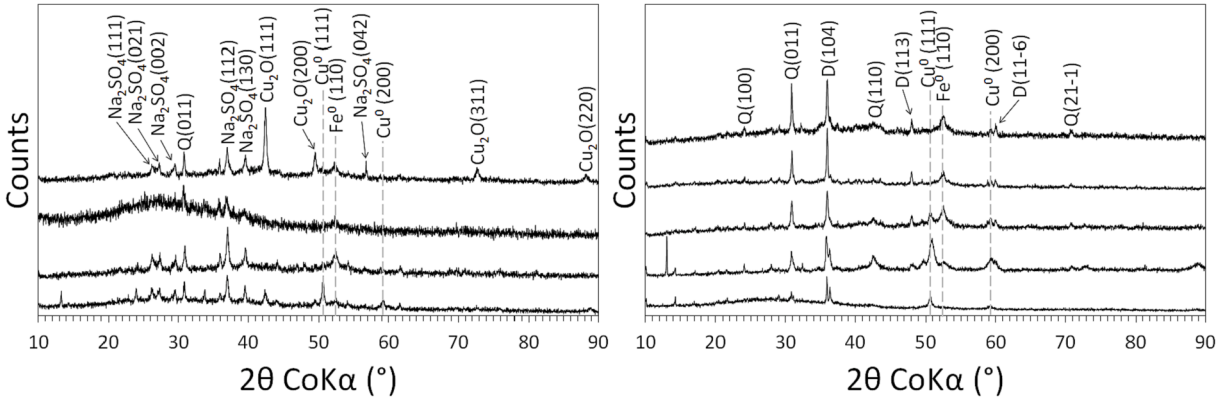

Fig. 5. XRD data recorded for the Cu bearing nanoparticles which were formed *via* the exposure of nZVI to Cu ore which had been first leached using 0.5 M H_2SO_4 (LHS) or CH_3COOH (RHS) and then neutralised using NaOH or $NaCO_3$ respectively. The profiles correspond to (stacked from bottom to top): NaOH concentrations (LHS) of 0.1, 0.2, 0.4 and 1.0 M; and $NaCO_3$ concentrations (RHS) of 0.1, 0.5, 1.0, 1.5 and 2.0 M. XRD data were not obtained for samples that were neutralised using a NaOH concentration of 0.01 M because the nZVI were visually observed to have fully dissolved.

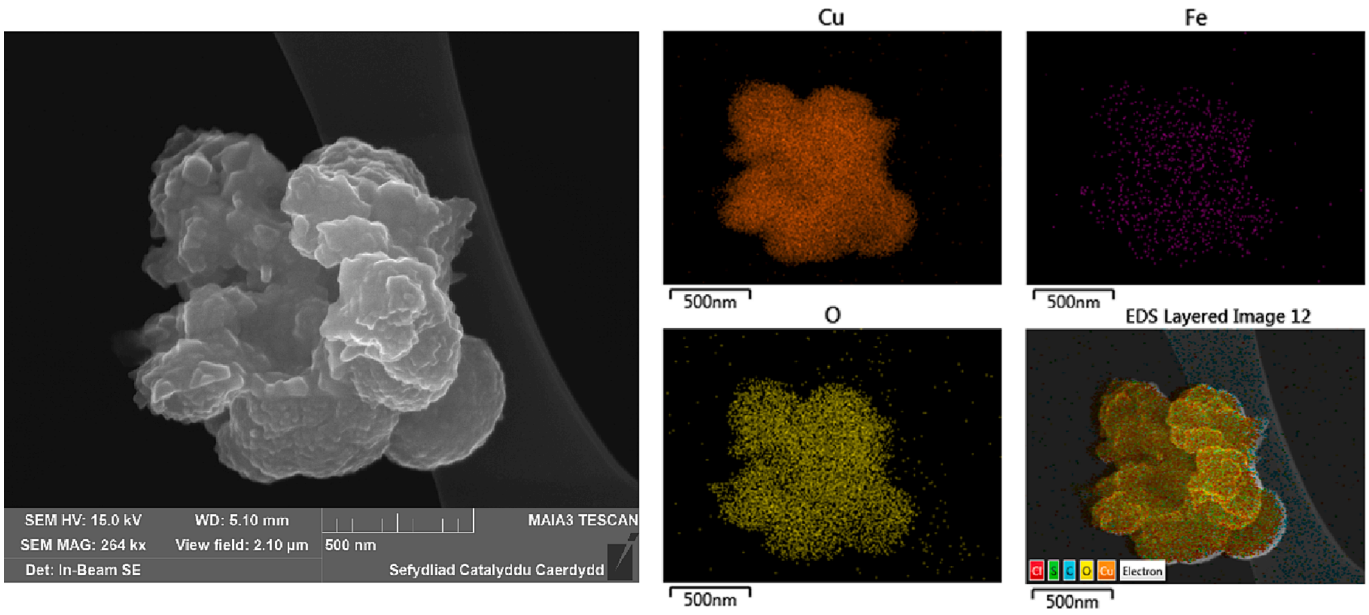

Fig. 6. FEG-SEM-EDS images and corresponding EDS maps for Cu, Fe and O of the Cu bearing nanoparticles which were formed *via* the exposure of nZVI to Cu ore which had first been leached using 0.5 M H_2SO_4 and then neutralised using 0.1 M NaOH. The nZVI (and entrained Cu nanoparticles) were then extracted using a magnetic field.

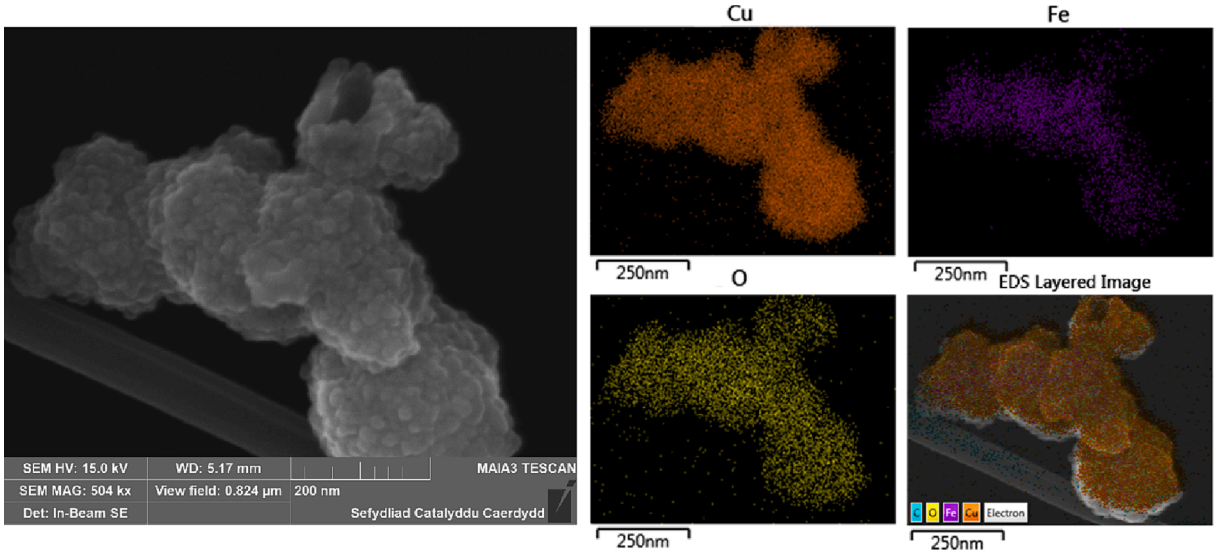

Fig. 7. FEG-SEM-EDS images and corresponding EDS maps for Cu, Fe, O and Na of the Cu bearing nanoparticles which were formed *via* the exposure of nZVI to Cu ore after it was leached using 0.5 M CH_3COOH and then neutralised using 0.1 M $NaCO_3$.

Table 3
Composition (by wt. %) as determined using FEG-SEM of the Cu bearing nanoparticles which were formed *via* the exposure of nZVI to Cu ore which had first been leached using 0.5 M H_2SO_4 or CH_3COOH and then neutralised using 0.1 M NaOH or $NaCO_3$ respectively. The data correlate to the EDS maps displayed in Figs. 6 and 7.

	0.5 M H_2SO_4 + 0.1 M NaOH	0.5 M CH_3COOH + 0.1 M $NaCO_3$
Element	Map (wt.%)	Map (wt.%)
O	16.89	11.13
Fe	0.47	11.27
Cl	0.41	0.00
Cu	81.70	77.60
S	0.43	0.00

H_2SO_4 or CH_3COOH and then neutralised using 0.1 M NaOH or $NaCO_3$ respectively (Table 3). In addition, they are observed to be relatively spherical, with 96 wt% and 99 wt% of particles recorded as < 50 nm diameter respectively (Table 4; Fig. 8). As such, the Cu-bearing nanoparticles in both instances can be described as of relatively similar morphology and size as the original as-formed nZVI (see Section 3.1.). This is an interesting result and suggests that the cementation reaction (Reaction (1)) proceeded by direct heterogeneous contact displacement (galvanic replacement): $Fe^0_{(s)} \rightarrow Fe^{2+}_{(aq)}$ with $Cu^{2+}_{(aq)} \rightarrow Cu^0_{(s)}$ (i.e. oxidation of nZVI coupled to the reductive precipitation of Cu in a 1:1 ratio which replicates the original morphology of the nZVI). Li et al (2021) suggest that the produced reduced copper may accelerate the further reaction of the nZVI. Recent work by Liu et al (Liu et al., 2022) indicates that galvanic exchange and the Kirkendall effect are important in determining the morphology of the resultant nCu during reaction of nZVI

Table 4
Physical and chemical properties of the Cu bearing nanoparticles which were formed *via* the exposure of nZVI to Cu ore after it was leached using 0.5 M H_2SO_4 or CH_3COOH and then neutralised using 0.1 M NaOH or $NaCO_3$ respectively. Ratio of Cu ore to nZVI was 25:1 (4.0 g/L nZVI: 100 g/L Cu ore).

Parameter	Analysis technique	Lixiviant and neutralisation agent	
		0.5 M H_2SO_4, 0.1 M NaOH	0.5 M CH_3COOH, 0.1 M $NaCO_3$
Particle size distribution (%)	FEG-SEM	0–10 nm: 4 10–25 nm: 52 25–50 nm: 42 >50 nm: 4	0–10 nm: 5 10–25 nm: 88 25–50 nm: 6 >50 nm: 1
Mean particle size (nm)	FEG-SEM	26	18
Median particle size (nm)	FEG-SEM	24	17
Composition	XRD	Cu^0, Cu_2O	Cu^0, Cu_2O
Maximum purity detected (wt. % Cu)	FEG-SEM-EDS	87.5	62.4
Nanoparticle shape	FEG-SEM	Spherical, rounded	Spherical, rounded

with Cu^{2+}. For example, the common absence of Fe corrosion products can be explained by the acidic conditions (generated by the acid leaching step prior to nZVI application) enabled Fe ions (produced in Reaction (1)) to remain in the aqueous phase rather than their precipitation as oxides/hydroxides.

Given that XRD analysis has recorded only two Cu phases (metallic and Cu_2O) (Fig. 5) and that Cu content detected using FEG-SEM were > 75 wt% for all systems studied (Table 3) it is likely that the majority of Cu was in metallic form, with a minor additional proportion from Cu_2O. This is in agreement with Fe-Cu half-cell standard electrode potentials which demonstrate that, from an electrochemical perspective, formation of Cu^0 is favourable.

4. Industrial/environmental implications

4.1. Use of nZVI as an agent for selective nCu synthesis

The nCu synthesis mechanism has been determined as predominantly *via* the cementation of aqueous Cu with nZVI, which comprises the heterogeneous reduction of Cu^{2+} to Cu^0 on nZVI with concurrent dissolution of Fe from the nZVI to form discrete Cu^0 nanoparticles (Reaction (1)). The reaction is spontaneous and results in the chemical reduction of Cu^{2+} to Cu^0 in a 1:1 M ratio with the oxidation of Fe^0 to Fe^{2+}. This simple one-pot methodology has been demonstrated herein for the conversion of Cu directly from malachite ore into Cu^0/Cu_2O nanoparticles of relatively high purity and well constrained particle size distribution. This methodology, the first proposed as a mass-production route for nCu, should be readily achievable based on the example of recent full-scale operation of an nZVI-based wastewater treatment plant (Li et al., 2017). From an economic perspective, using nZVI as the reductant in the production of the nCu in turn requires the application of a suitable method for the mass-production of the nZVI. However, large-scale production has already been developed for nZVI due to its use in large quantities in environmental remediation. Synthesis routes include the "top down" methods of lithographic grinding, precision milling and "bottom up" methods including chemical and carbothermal reduction, electrochemical and green synthesis methods (Nikam et al., 2014). The wholesale cost for nZVI currently ranges from £500-2000/t ($680–1400/t) compared to approximately 10,000 United States Dollars (USD)/t for bulk orders of Cu nanoparticles which comprise relatively low purity and unconstrained particle size distributions (PSD) (www.alibaba.com) to upwards of approximately 50,000 USD/t for well constrained nanopowder (e.g. (www.sigmaaldrich.com).The process is reliant on only minor quantities of low-cost additional reagents (namely the optimal conditions for the initial Cu ore leaching step was determined to be 0.5 M H_2SO_4 (approximately 5 % concentration by volume). It is therefore likely that this overall process will exhibit favourable economics in terms of reagent consumption. It will also potentially unlock an entirely new method of Cu mining (discussed in Section 4.2.) with potentially dramatically more favourable economic margins and environmental benefits.

Given that the most significant likely reagent cost will be the nZVI it is also likely that this cost could further decrease in the future as global use of nZVI technology continues to increase (particular in the contaminated land remediation but also in emerging technologies such as herein). The price differential between bulk iron and copper may provide sufficient economic and "circular economy" drivers for the grinding/milling routes. For example, currently scrap steel in the UK is approximately £450/t ($540/t) (London Metal Exchange) and there are also several potential scenarios whereby nZVI could be made cheaply and sustainably using waste materials/waters. Key examples include

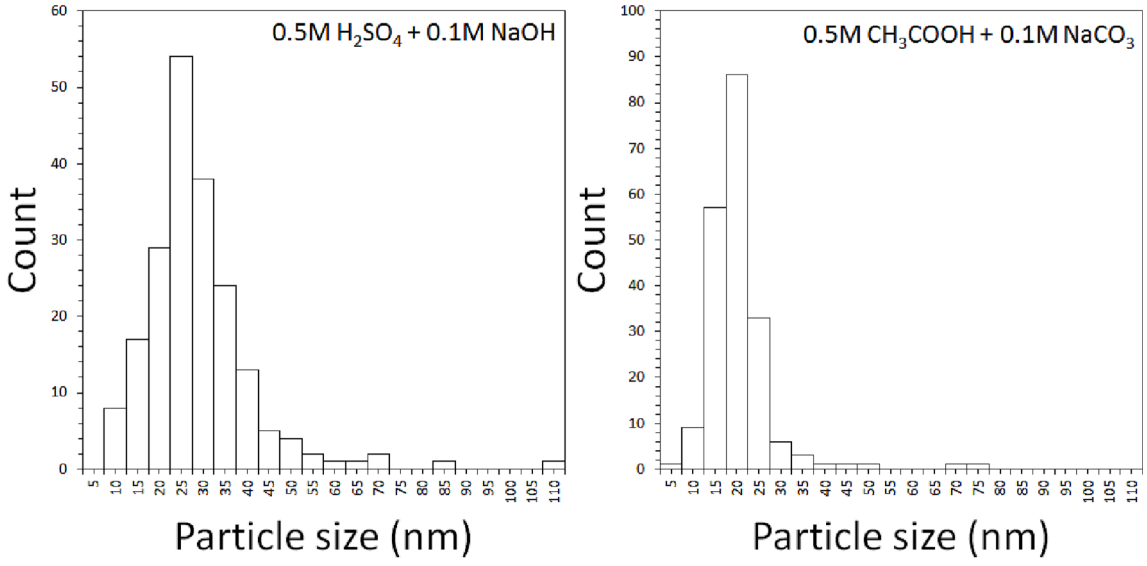

Fig. 8. Particle size distribution of the Cu bearing nanoparticles (n = 200; data collected using analysis of FEG-SEM images) which were formed *via* the exposure of nZVI to Cu ore after it was leaching using 0.5 M H_2SO_4 or CH_3COOH and then neutralised using 0.1 M NaOH or $NaCO_3$ respectively. Ratio of Cu ore to nZVI was 25:1 (4.0 g/L nZVI: 100 g/L Cu ore).

acid mine drainage, pickling sludge and steel smelting waste.

It is also significant to note that this proposed process could enable the substantial economic benefit of valorising ore directly to a nanomaterial product. Ore cut-off grades are currently considered based on the premise of the conversion of ore to concentrate, withthe metallurgical processing of ore concentrates into a metallic sheet/ingot often outsourced to a different mineral processing company. Given this, the new proposed "direct conversion of ore to high value product" could therefore unlock a wide range of ore deposits which are currently economically unviable.

4.2. Towards green mining technology for sustainable nCu mass production

Precision Mining is a recently introduced concept (Crane and Sapsford, 2018 Jul) which can be defined as a methodology whereby a target resource (e.g. a metal) is selectively removed from it host material (e.g. an ore body, waste or wastewater) *in situ* and then transported to the surface for recovery. Precision Mining is in principle, a dramatically more environmentally compatible mining process than conventional approaches (namely physical excavation) due to the fact that such resource recovery could be achieved with minimal disturbance to the host material/environment and would produce minimal waste. In order to achieve this, consideration should be made of the environmental compatibility/toxicity or any reagents and associated engineering process.Such information should also be evaluated against efficacy and selectivity of both the metal leaching and nanoparticle recovery process.

Herein, the organic acid lixiviant CH_3COOH was investigated because reagent biodegradability is important in limiting the potential impact of any unintended loss during application (Crane and Stewart, 2021). CH_3COOH was demonstrated as suitable lixiviant (through comparison with H_2SO_4) dissolving Cu even when applied at relatively low concentrations (0.5 M). This enabled the target metal to be dissolved whilst exerting minimal chemical perturbation of the host media. Furthermore, the results demonstrate that a strong and weak base can be applied prior to nZVI addition to partially neutralise H_2SO_4 or CH_3COOH and create favourable pH conditions for selective nCu precipitation but with the additional benefit of further lowering their acidity.

nZVI has h been demonstrated as selective for Cu and is a relatively environmentally benign reductant to use at large scale within the environment. Whilst not without impact, its environmental toxicity and transport is likely to be mitigated by its tendency to oxidise and subsequently aggregate rapidly in the physicochemical conditions encountered *in situ* (Lefevre et al., 2016). This compares favourably with other aqueous reductants that have been used for nCu production, that could feasibly be injected into the ground, but whose toxicity is high, such as hydrazine hydrate (Su et al., 2007 Oct 11) or sodium borohydride (Huang et al., 2012).

In addition, results demonstrate that because product nCu was entrained with residual (super)paramagnetic nZVI (Borglin et al., 2000), it was efficiently recovered using an externally applied magnetic field. The exact mechanism of nCu removal remains unclear. However, given that nCu is known to exhibit ferromagnetic and (giant)paramagnetic properties (typically when in the size range of < 500 nm) (Manukyan et al., 2019) it may have been removed directly. Future work will seek to understand this potential beneficial magnetic property. FEG-SEM analysis confirmed that the nCu precipitate was in the form of discrete nanoparticles, and as such likely to be able to be removed easily from the nZVI by techniques such as centrifugation (e.g. (Akbulut et al., 2012).

The application of nZVI for selective nCu synthesis could also be coupled with *ex situ* ore processing. In recent years "in pulp" methods (such as resin in pulp (RIP)) have increasingly been used for the recovery of Cu from low-grade ores and for improving recovery efficacy from Cu leach slurries that have poor filterability and/or settling characteristics. The chief advantage is elimination of the need for high liquid–solid ratios when undertaking hydrometallurgical operations and thus saving the considerable cost associated with slurry filtration and treatment of the filtrate (Nicol and Zainol, 2003). Despite such benefits, RIP remains an underutilised technology which is primarily due to concerns over the durability and reusability of such resins (Udayar et al., 2011). Instead "nZVI in pulp" could realise the advantages of in pulp methods, but with the added benefit of the direct conversion of Cu to a valuable nanoproduct. Separation of the pulp from the product nanoparticles might also conceivably be achieved using magnetic separation (if unreacted nZVI remains entrained with the Cu product), the use of deflocculants (such as $Na_4P_2O_7$) or *via* physical methods, such as sonication.

5. Conclusions

Previous studies into the application on nZVI for Cu^{2+} removal have focussed on its application for environmental remediation and wastewater treatment. Herein, we have provided proof of concept for a new methodology that utilises this chemistry for the selective conversion of a metal from its ore directly into a high value nanomaterial product. Malachite ore, a globally significant mineral and commodity, was first exposed to 0.5 M H_2SO_4 or CH_3COOH solutions which were then partially neutralised using 0.01–0.5 M NaOH or $NaCO_3$ solutions respectively. Pregnant solutions were then exposed to nZVI, with the resultant surface bound precipitate recovered using a magnetic field. The following can be concluded:

1) Application of nZVI results in the rapid (<240 s) cementation of copper as discrete Cu^0/Cu_2O nanoparticles, possibly representing a direct method of mass production of nCu directly from ores within stirred leach tanks or for potential application *in situ*. This would avoid the need to physically excavate the ore and therefore potentially realise a dramatically less energy-intensive approach to Cu mining.
2) Comparison of strong to weak acid/base combinations demonstrated that 0.5 M H_2SO_4 was more effective than equimolar solutions of CH_3COOH for the dissolution of Cu from its malachite ore (1:10 SL ratio). Average Cu dissolution was 67.4 compared to 16.16 wt% respectively but following nZVI addition both systems produced Cu/Cu_2O nanoparticles of similar composition.
3) nZVI was selective for Cu removal from the pregnant leachate. Analysis of metal proportions in the "removed phase" determined Cu at 94.9 and 97.5 wt% for the H_2SO_4 and CH_3COOH systems respectively (Table 2).
4) XRD analysis of the magnetically extracted precipitate recorded the presence of Cu^0 which confirmed that the removal mechanism of aqueous Cu was *via* cementation.

FEG-SEM-EDS analysis of the magnetically extracted precipitate determined that Cu was in the form of discrete spherical nanoparticles (mean particle size 18–26 nm) which were found to be entrained within the nZVI. The SEM-EDS analyses also revealed that under the experimental conditions used, galvanic replacement of Fe with Cu was pseudomorphic.

Overall, the results demonstrate nZVI as highly selective for the rapid synthesis of discrete Cu^0/Cu_2O nanoparticles from acid leached malachite ore, with facile recovery of product nanoparticle agglomerations with unreacted nZVI achieved using a magnetic field. The technique holds great promise as a means of mass production of the nCu that will be required for many of this century's largest technological challenges. The process could also readily be coupled with more sustainable next generation mining technologies such as "precision" and "keyhole" mining" and thus could represent an new paradigm for the conversion of low-grade Cu ore and Cu bearing waste to valuable nanoparticulate Cu-based materials.

CRediT authorship contribution statement

R.A. Crane: Conceptualization, Methodology, Software, Validation, Formal analysis, Writing – original draft. **D.J. Sapsford:** Conceptualization, Formal analysis, Resources, Writing – review & editing, Project administration, Funding acquisition.

Declaration of Competing Interest

The authors declare that they have no known competing financial interests or personal relationships that could have appeared to influence the work reported in this paper.

Data availability

Data will be made available on request.

Acknowledgements

We would like to thank Mr Jeff Rowlands and Mr Marco Santonastaso and from the School of Engineering, Cardiff University for their technical support. We would also like to thank Dr Robert Bowell from SRK for valuable input. We would also like to thank Dr Thomas Davies from the Cardiff Catalysis Institute and the Cardiff Electron Microscopy Facility for the HRTEM-EDS and FEG-SEM-EDS analysis and Dr David Morgan from the School of Chemistry, Cardiff University for the BET surface area analysis. This work was financially supported by the Natural Environment Research Council (grant number: NE/L013908/1).

References

Akbulut, O., Mace, C.R., Martinez, R.V., Kumar, A.A., Nie, Z., Patton, M.R., Whitesides, G.M., 2012. Separation of nanoparticles in aqueous multiphase systems through centrifugation. Nano Lett. 12 (8), 4060–4064.

Ameh, T., Sayes, C.M., 2019. The potential exposure and hazards of copper nanoparticles: a review. Environ. Toxicol. Pharmacol. 71, 103220.

Baalousha, M., 2009. Aggregation and disaggregation of iron oxide nanoparticles: influence of particle concentration, pH and natural organic matter. Sci. Tot. Environ. 407, 2093–2101.

Baláž, M., Tešinský, M., Marquardt, J., Škrobian, M., Daneu, N., Rajňák, M., Baláž, P., 2020. Synthesis of copper nanoparticles from refractory sulfides using a semi-industrial mechanochemical approach. Adv. Powder Technol. 31 (2), 782–791.

Bingöl, D., Canbazoğlu, M., 2004. Dissolution kinetics of malachite in sulfuric acid. Hydrometall. 72 (1), 159–165.

Borda, F.L.G., de Oliveira, S.J.R., Lazaro, L.M.S.M., Leiróz, A.J.K., 2018. Experimental investigation of the tribological behavior of lubricants with additive containing copper nanoparticles. Tribol. Int. 117, 52–58.

Borglin, S.E., Moridis, G.J., Oldenburg, C.M., 2000. Experimental studies of the flow of ferrofluid in porous media. Transp. Porous Media 41 (1), 61–80.

Crane, R.A., Pullin, H, Macfarlane, J., Silion, M., Popescu, I.C., Andersen, M., Calen, V., Scott, T.B. Field application of iron and iron–nickel nanoparticles for the ex situ remediation of a uranium-bearing mine water effluent. J. Environ. Eng. 141 (8), 04015011.

Crane, R.A., Pullin, H., Scott, T.B. The influence of calcium, sodium and bicarbonate on the uptake of uranium onto nanoscale zero-valent iron particles. Chem. Eng. J. 277, 252-259.

Crane, R.A., Sapsford, D.J., 2018 Aug. Sorption and fractionation of rare earth element ions onto nanoscale zerovalent iron particles. Chem. Eng. J. 1 (345), 126–137.

Crane, R.A., Sapsford, D.J., 2018 Jul. Towards "Precision Mining" of wastewater: Selective recovery of Cu from acid mine drainage onto diatomite supported nanoscale zerovalent iron particles. Chemosphere 1 (202), 339–348.

Crane, R.A., Sapsford, D.J., 2018 Apr. Selective formation of copper nanoparticles from acid mine drainage using nanoscale zerovalent iron particles. J. Hazard. Mater. 5 (347), 252–265.

Crane, R.A., Sapsford, D.J., 2018 Sep. Towards greener lixiviants in value recovery from mine wastes: efficacy of organic acids for the dissolution of copper and arsenic from legacy mine tailings. Minerals. 8 (9), 383.

Crane, R.A., Scott, T.B., 2013. The effect of vacuum annealing of magnetite and zero-valent iron nanoparticles on the removal of aqueous uranium. J. Nanotechnol. 2013.

Crane, R.A., Stewart, J., 2021. Selective leaching of ecotoxic metals from lime dosing plant metalliferous ochre using acid mine drainage and organic acids. Miner. Eng. 160, 106687.

Dimkpa, C.O., McLean, J.E., Britt, D.W., Anderson, A.J., 2012. Bioactivity and biomodification of Ag, ZnO, and CuO nanoparticles with relevance to plant performance in agriculture. Ind. Biotechnol. 8 (6), 344–357.

Elouali, S., Bloor, L.G., Binions, R., Parkin, I.P., Carmalt, C.J., Darr, J.A., 2012. Gas sensing with nano-indium oxides (In2O3) prepared via continuous hydrothermal flow synthesis. Langmuir 28 (3), 1879–1885.

EPA, 1996. Microwave assisted acid digestion of siliceous and organically based matrices, s.l.: EPA method 3052 – 1. URL: https://www.epa.gov/sites/production/files/2015-12/documents/3052.pdf.

Foley, J.A., Ramankutty, N., Brauman, K.A., Cassidy, E.S., Gerber, J.S., Johnston, M., Mueller, N.D., O'Connell, C., Ray, D.K., West, P.C., Balzer, C., Bennett, E.M., Carpenter, S.R., Hill, J., Monfreda, C., Polasky, S., Rockström, J., Sheehan, J., Siebert, S., et al., 2011. Solutions for a cultivated planet. Nature 478, 337–342.

Gawande, M.B., Goswami, A., Felpin, F.X., Asefa, T., Huang, X., Silva, R., Zou, X., Zboril, R., Varma, R.S., 2016. Cu and Cu-based nanoparticles: synthesis and applications in catalysis. Chem. Rev. 116 (6), 3722–3811.

Glavee, G.N., Klabunde, K.J., Sorensen, C.M., Hadjipanayis, G.C., 1995. Chemistry of borohydride reduction of iron(II) and iron(III) ions in aqueous and nonaqueous media, formation of nanoscale Fe, FeB and Fe2B powders. Inorg. Chem. 34, 28–35.

González-García, Y., Cárdenas-Álvarez, C., Cadenas-Pliego, G., Benavides-Mendoza, A., Cabrera-de-la-Fuente, M., Sandoval-Rangel, A., Valdés-Reyna, J., Juárez-Maldonado, A., 2021. Effect of three nanoparticles (Se, Si and Cu) on the bioactive compounds of bell pepper fruits under saline stress. Plants 10 (2), 217.

Guan, X., Gao, X., Avellan, A., Spielman-Sun, E., Xu, J., Laughton, S.N., Yun, J., Zhang, Y., Bland, G.D., Zhang, Y., Zhang, R., 2020. CuO nanoparticles alter the rhizospheric bacterial community and local nitrogen cycling for wheat grown in a calcareous soil. Environ. Sci. Tech.

Gupta, K., Bersani, M., Darr, J.A., 2016. Highly efficient electro-reduction of CO 2 to formic acid by nano-copper. J. Mater. Chem. A 4 (36), 13786–13794.

https://openknowledge.worldbank.org/handle/10986/30317 (Accessed 23/02/23).

Huang, C.C., Lo, S.L., Lien, H.L., 2012. Zero-valent copper nanoparticles for effective dechlorination of dichloromethane using sodium borohydride as a reductant. Chem. Eng. J. 203, 95–100.

Hudson-Edwards, K.A., Jamieson, H.E., Lottermoser, B.G., 2011 Dec 1. Mine wastes: past, present, future. Elements 7 (6), 375–380.

Ingle, A.P., Duran, N., Rai, M., 2014. Bioactivity, mechanism of action, and cytotoxicity of copper-based nanoparticles: a review. Appl. Microbiol. Biotechnol. 98 (3), 1001–1009.

Jardón-Maximino, N., Pérez-Alvarez, M., Cadenas-Pliego, G., Lugo-Uribe, L.E., Cabello-Alvarado, C., Mata-Padilla, J.M., Barriga-Castro, E.D., 2021. Synthesis of copper nanoparticles stabilized with organic ligands and their antimicrobial properties. Polymers 13 (17), 2846.

Jardón-Maximino, N., Cadenas-Pliego, G., Ávila-Orta, C.A., Comparán-Padilla, V.E., Lugo-Uribe, L.E., Pérez-Alvarez, M., Tavizón, S.F., Santillán, G.D.J.S., 2021. Antimicrobial property of polypropylene composites and functionalized copper nanoparticles. Polymers 13 (11), 1694.

Jardón-Maximino, N., Pérez-Alvarez, M., Sierra-Ávila, R., Ávila-Orta, C.A., Jiménez-Regalado, E., Bello, A.M., González-Morones, P. and Cadenas-Pliego, G., 2018. Oxidation of copper nanoparticles protected with different coatings and stored under ambient conditions. J. Nanomater., 2018.

Jones, J.P., Prakash, G.S., Olah, G.A., 2014. Electrochemical CO2 reduction: recent advances and current trends. Isr. J. Chem. 54 (10), 1451–1466.

Karabelli, D., Üzüm, C., Shahwan, T., Eroglu, A.E., Scott, T.B., Hallam, K.R., Lieberwirth, I., 2008. Batch removal of aqueous Cu2+ ions using nanoparticles of zero-valent iron: a study of the capacity and mechanism of uptake. Ind. Eng. Chem. Res. 47 (14), 4758–4764.

Lefevre, E., Bossa, N., Wiesner, M.R., Gunsch, C.K., 2016. A review of the environmental implications of in situ remediation by nanoscale zero valent iron (nZVI): behavior, transport and impacts on microbial communities. Sci. Total Environ. 565, 889–901.

Li, S., Wang, W., Yan, W., Zhang, W.X., 2014. Nanoscale zero-valent iron (nZVI) for the treatment of concentrated Cu (II) wastewater: a field demonstration. Environ. Sci. Processes Impacts 16 (3), 524–533.

Li, S., Wang, W., Liang, F., Zhang, W.X., 2017. Heavy metal removal using nanoscale zero-valent iron (nZVI): Theory and application. J. Hazard. Mater. 322, 163–171.

Liu, A., Fu, J., Liu, J., Zhang, W., 2022. Copper Nanostructure Genesis via Galvanic Replacement and Kirkendall Growth from Nanoscale Zero-Valent Iron. ACS ES&T Water 2 (8), 1353–1359.

London Metal Exchange https://www.lme.com/en-GB/Metals/Ferrous/Steel-Scrap#tabIndex=0 (accessed 23-02-23).

Manukyan, A., Gyulasaryan, H., Kocharian, A., Estiphanos, M., Bernal, O., Sharoyan, E., 2019. Ferromagnetism and giant paramagnetism of copper nanoparticles in Cum/C nanocomposites. J. Magn. Magn. Mater. 488, 165336.

Martens, E., Prommer, H., Sprocati, R., Sun, J., Dai, X., Crane, R., Jamieson, J., Tong, P. O., Rolle, M., Fourie, A. Toward a more sustainable mining future with electrokinetic in situ leaching. Sci. Adv. 2021 Apr 1;7(18):eabf9971.

Mueller, N.D., Gerber, J.S., Johnston, M., Ray, D.K., Ramankutty, N., Foley, J.A., 2012. Closing yield gaps through nutrient and water management. Nature 490, 254–257.

Neupane, M.P., Kim, Y.K., Park, I.S., Kim, K.A., Lee, M.H., Bae, T.S., 2009. Temperature driven morphological changes of hydrothermally prepared copper oxide nanoparticles. Surf. Interface Anal.: Int. J. Devoted Devel. Appl. Tech. Anal. Surf., Interfaces Thin Films 41 (3), 259–263.

Ngo, Q.B., Dao, T.H., Nguyen, H.C., Tran, X.T., Van Nguyen, T., Khuu, T.D., Huynh, T.H., 2014. Effects of nanocrystalline powders (Fe, Co and Cu) on the germination, growth, crop yield and product quality of soybean (Vietnamese species DT-51). Adv. Nat. Sci. Nanosci. Nanotechnol. 5 (1), 015016.

Nicol, M.J., Zainol, Z., 2003. The development of a resin-in-pulp process for the recovery of nickel and cobalt from laterite leach slurries. Int. J. Miner. Process. 72 (1), 407–415.

Nikam, A.V., Arulkashmir, A., Krishnamoorthy, K., Kulkarni, A.A., Prasad, B.L.V., 2014. pH-dependent single-step rapid synthesis of CuO and Cu2O nanoparticles from the same precursor. Cryst. Growth Des. 14 (9), 4329–4334.
Ogunsona, E.O., Muthuraj, R., Ojogbo, E., Valerio, O., Mekonnen, T.H., 2020. Engineered nanomaterials for antimicrobial applications: a review. Appl. Mater. Today 18, 100473.
Outokesh, M., Hosseinpour, M., Ahmadi, S.J., Mousavand, T., Sadjadi, S., Soltanian, W., 2011. Hydrothermal synthesis of CuO nanoparticles: study on effects of operational conditions on yield, purity, and size of the nanoparticles. Ind. Eng. Chem. Res. 50 (6), 3540–3554.
Pérez-Alvarez, M., Cadenas-Pliego, G., Pérez-Camacho, O., Comparán-Padilla, V.E., Cabello-Alvarado, C.J., Saucedo-Salazar, E., 2021. Green synthesis of copper nanoparticles using cotton. Polymers 13 (12), 1906.
Ponmurugan, P., Manjukarunambika, K., Elango, V., Gnanamangai, B.M., 2016. Antifungal activity of biosynthesised copper nanoparticles evaluated against red root-rot disease in tea plants. J. Exp. Nanosci. 11 (13), 1019–1031.
Scott, T.B., Dickinson, M., Crane, R.A., Riba, O., Hughes, G.M., Allen, G.C. The effects of vacuum annealing on the structure and surface chemistry of iron nanoparticles. J. Nanoparticle Res. 12 (5), 1765-1775.
Seredkin, M., Zabolotsky, A., Jeffress, G., 2016 Dec. In situ recovery, an alternative to conventional methods of mining: exploration, resource estimation, environmental issues, project evaluation and economics. Ore Geol. Rev. 1 (79), 500–514.
Slotte, M., Zevenhoven, R., 2017. Energy efficiency and scalability of metallic nanoparticle production using arc/spark discharge. Energies 10 (10), 1605.
Stefanowicz, T., Osińska, M., Napieralska-Zagozda, S., 1997 Nov 1. Copper recovery by the cementation method. Hydrometall. 47 (1), 69–90.
Su, X., Zhao, J., Bala, H., Zhu, Y., Gao, Y., Ma, S., Wang, Z., 2007 Oct 11. Fast synthesis of stable cubic copper nanocages in the aqueous phase. J. Phys. Chem. C 111 (40), 14689–14693.
Tamilvanan, A., Balamurugan, K., Vijayakumar, M., 2019. Effects of nano-copper additive on performance, combustion and emission characteristics of Calophyllum inophyllum biodiesel in CI engine. J. Therm. Anal. Calorim. 136 (1), 317–330.
Udayar, T., Kotze, M.H., Yahorava, V. (2011). Recovery of uranium from dense slurries via resin-in-pulp. In: Proceedings of the 6th Southern African Base Metals Conference (p. 49).
Vidyasagar, C.C., Naik, Y.A., Venkatesha, T.G., Viswanatha, R., 2012. Solid-state synthesis and effect of temperature on optical properties of CuO nanoparticles. Nano-Micro Letters 4 (2), 73–77.
Vilardi, G., 2019. Mathematical modelling of simultaneous nitrate and dissolved oxygen reduction by Cu-nZVI using a bi-component shrinking core model. Powder Technol. 343, 613–618.
Wang, C.B., Zhang, W.-X., 1997. Synthesizing nanoscale iron particles for rapid and complete dechlorination of TCE and PCBs. Environ. Sci. Tech. 31, 2154–2156.
www.alibaba.com (Accessed 23/02/23) “copper nanopowder” search function.
Copper nanopowder, <60-80 nm (BET), ≥99.5% trace metals basis. Product number: 774103-5G; URL: www.sigmaaldrich.com (Accessed 23/02/23).
Xie, H., Wang, T., Liang, J., Li, Q., Sun, S., 2018. Cu-based nanocatalysts for electrochemical reduction of CO2. Nano Today 21, 41–54.
Yuan, G.Q., Jiang, H.F., Lin, C., Liao, S.J., 2007. Shape-and size-controlled electrochemical synthesis of cupric oxide nanocrystals. J. Cryst. Growth 303 (2), 400–406.
Zhang, Y., Zhu, P., Li, G., Zhao, T., Fu, X., Sun, R., Zhou, F., Wong, C.P., 2014. Facile preparation of monodisperse, impurity-free, and antioxidation copper nanoparticles on a large scale for application in conductive ink. ACS Appl. Mater. Interfaces 6 (1), 560–567.
Zhu, J., Li, D., Chen, H., Yang, X., Lu, L., Wang, X., 2004. Highly dispersed CuO nanoparticles prepared by a novel quick-precipitation method. Mater. Lett. 58 (26), 3324–3327.